Available online at www.sciencedirect.com
ScienceDirect
European Journal of Medicinal Chemistry 43 (2008) 621–632
EUROPEAN JOURNAL OF MEDICINAL CHEMISTRY
http://www.elsevier.com/locate/ejmech

Original article

Class II-selective histone deacetylase inhibitors. Part 2: Alignment-independent GRIND 3-D QSAR, homology and docking studies

Rino Ragno [a,*], Silvia Simeoni [a], Dante Rotili [a], Antonella Caroli [a], Giorgia Botta [a], Gerald Brosch [b], Silvio Massa [c], Antonello Mai [a,**]

[a] *Istituto Pasteur – Fondazione Cenci Bolognetti, Dipartimento di Studi Farmaceutici, Università degli Studi di Roma "La Sapienza", P.le A. Moro 5, 00185 Roma, Italy*
[b] *Department of Molecular Biology, Innsbruck Medical University, Peter-Mayr-Strasse 4b, 6020 Innsbruck, Austria*
[c] *Dipartimento Farmaco Chimico Tecnologico, Università degli Studi di Siena, via A. Moro, 53100 Siena, Italy*

Received 13 February 2007; received in revised form 10 May 2007; accepted 14 May 2007
Available online 27 May 2007

Abstract

(Aryloxopropenyl)pyrrolyl hydroxamates were recently reported by us as first examples of class II-selective HDAC inhibitors and can be useful tools to probe the biology of such enzymes. Molecular modelling and 3-D QSAR studies have been performed on a series of 25 (aryloxopropenyl)pyrrolyl hydroxamates to gain insights about their activity and selectivity against both maize HD1-B and HD1-A, two enzymes homologous of mammalian class I and class II HDACs, respectively. The studies have been accomplished by calculating alignment-independent descriptors (GRIND descriptors) using the ALMOND software. Highly descriptive and predictive 3-D QSAR models were obtained using either class I or class II inhibitory activity displaying r^2/q^2 values of 0.96/0.81 and 0.98/0.85 for HD1-B and HD1-A, respectively. A deeper inspection revealed that in general a bent molecular shape structure is a prerequisite for HD1-A-selective inhibitory activity, while straight shape molecular skeleton leads to selective HD1-B compounds. The same conclusions could be achieved by molecular docking studies of the most selective inhibitors.
© 2007 Elsevier Masson SAS. All rights reserved.

Keywords: Histone deacetylation; HDAC inhibitors; Class selectivity; GRIND descriptors; ALMOND; 3-D QSAR

1. Introduction

Histone deacetylase (HDAC) and histone acetyltransferase (HAT) are key enzymes involved in histone acetylation, which play an important role in regulation of gene expression [1]. HAT-promoted acetylation is related with nucleosomal relaxation and gene transcription, HDAC-promoted deacetylation with tightness of nucleosomal integrity and gene silencing [2]. HDAC inhibitors can reactivate gene expression, and are potent inducers of growth arrest, differentiation, or apoptotic cell death in a variety of transformed cells in culture and in tumor bearing animals [3]. Mammalian HDACs were grouped into three classes, according to their homology with *Saccharomyces cerevisiae* transcriptional regulators RPD3 (class I HDACs), HDA-1 (class II HDACs), or Sir2 (class III HDACs, sirtuins) [4,5]. Another eukaryote deacetylase, maize HD2, is structurally different from mammalian HDACs and was attributed to a class of its own [6]. Class I (HDAC1–3,8, and in Part 11) and II (HDAC4–7,9,10) HDACs are Zn^{+2}-dependent deacetylases, and are sensitive to known HDAC inhibitors such as hydroxamates (*i.e.*, trichostatin A (TSA), suberoylanilide hydroxamic acid (SAHA), scriptaid, oxamflatin, NVP-LAQ824, cyclic hydroxamic acid-containing peptides (CHAPs), tubacin),

* Corresponding author. Tel.: +39 6 4991 3152; fax: +39 6 491491.
** Corresponding author. Tel.: +39 6 4991 3392; fax: +39 6 491491.
E-mail addresses: rino.ragno@uniroma1.it (R. Ragno), antonello.mai@uniroma1.it (A. Mai).

0223-5234/$ - see front matter © 2007 Elsevier Masson SAS. All rights reserved.
doi:10.1016/j.ejmech.2007.05.004

cyclic peptides (*i.e.*, trapoxin, apicidin, FK-228), short chain fatty acids (sodium butyrate, sodium valproate), and 2′-aminoanilides (MS-275, acetyldinaline, histacin) [3]. Class II HDACs were further subdivided into two subclasses, IIa (HDAC4,5,7,9) and IIb (HDAC6,10), according to their sequence homology, subcellular localization, tissue expression, and domain organization [7]. Class III HDACs have a NAD^+-dependent mechanism of deacetylation, they are structurally and evolutionary unrelated to the class I and II proteins and are not sensitive to HDAC inhibitors [8].

In cells, class I and class II HDACs are recruited as part of multicomponent repressor complexes, such as *N*-CoR/SMRT, Sin3, NuRD, and CoREST complexes, and a large number of transcription factors were shown to bind to corepressor complexes as a means of regulating transcription. Moreover, interaction between different HDAC isozymes (*i.e.*, HDAC4, 5, or 7 and HDAC3, or HDAC6 and SIRT2) were described to regulate transcription or microtubule destabilization [9,10].

Most of known HDAC inhibitors do not show selectivity for one class (or subclass) of these proteins, the only exceptions being VPA [11], FK-228 [12] 2′-aminoanilide-based inhibitors [13], SB-429201 and SB-379278-A [14] (class I-selective compounds), and tubacin [15] and thiol-based derivatives [16] as HDAC6-selective inhibitors. Moreover, class IIb HDAC6 and HDAC10 have been found to be resistant to trapoxin, CHAPs, and sodium butyrate [17]. Further development of new small molecules with the specificity to selectively inhibit only a (sub)class of the HDAC family is a very attractive goal to pursue, because such compounds could be useful tools to elucidate the role of a particular (sub)class of HDACs in different protein complexes.

In 2003 a new series of pyrrole-containing compounds, namely (aryloxopropenyl)pyrrolyl hydroxamides, were reported by us as class II-selective HDAC inhibitors [18]. These small molecules were discovered by chemical manipulation performed on the aroyl-pyrrolyl-hydroxamide (APHA) template previously described by us [19–23]. To evaluate the class I/class II selectivity of (aryloxopropenyl)pyrrolyl hydroxamides, the new derivatives were tested against HD1-B [24,25] and HD1-A enzymes [26,27], two maize deacetylases that are homologues of mammalian class I and class II HDACs, respectively. The maize system offers the advantage of the use of completely separated enzyme active forms, while human HDACs act as multiprotein and, in some cases, multi-HDAC containing complexes in their active forms [28]. Nevertheless the maize enzymes share acceptable sequence similarities with the human homologues enzymes (see Section 5 and Supplementary data) and being much easier to purify we have decided to use the maize systems as working horse to screen newly synthesized compounds.

By this screening, properly substituted derivatives among the prepared and tested (aryloxopropenyl)pyrrolyl hydroxyamides **1–25** (Fig. 1) were shown to be highly selective against the class II HDAC homologous HD1-A (Table 1) [29].

In parallel with the chemistry/biochemistry [29] 3-D QSAR studies on the designed (aryloxopropenyl)pyrrolyl hydroxyamides **1–25** were performed to gain insights about their activity and selectivity on HD1-B and HD1-A enzymes. These studies were accomplished by calculating alignment-independent descriptors using the ALMOND 3.2.0a software [30]. These GRID independent descriptors (GRIND) represent the most important GRID interactions [31] as a function of the distance instead of the position of each grid point: it means that they are insensitive to the position and orientation of the molecular structures in the space [30,32]. Starting from simulated annealing generated conformations the training set of the (aryloxopropenyl)pyrrolyl hydroxyamides **1–25** were correlated with the 3-D GRIND descriptors to achieve highly self-consistent 3-D QSAR models. The HD1-B *vs* the HD1-A (and vice versa) selectivity of newly synthesized (aryloxopropenyl)pyrrolyl hydroxyamides were correctly predicted by the 3-D QSAR models. Further molecular docking studies, using homology models of the HD1-B and HD1-A enzymes supported that the overall molecular geometry is of crucial importance for HDAC class I- or class II-selective inhibition.

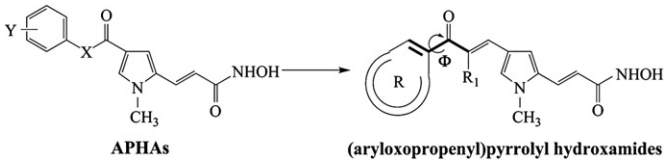

Fig. 1. From aroyl-pyrrolyl-hydroxamides (APHAs) to (aryloxopropenyl)-pyrrolyl hydroxamides **1–25**.

2. Chemistry

Synthetic methods as well as chemical and physical data for compounds **1–21** were reported in Part 1 of this work [29]. The missing compounds **22–25** were obtained by reaction between ethyl 3-(4-formyl-1-methyl-1*H*-pyrrol-2-yl)-2-propenoate **26** and the appropriate methyl-heteroaryl-ketone dissolved in ethanol in the presence of sodium ethoxide. The crude ethyl 3-[4-(3-heteroaryl-3-oxopropen-1-yl)-1-methyl-1*H*-pyrrol-2-yl]-2-propenoates were hydrolysed in alkaline medium to furnish the corresponding (heteroaryloxopropenyl)-pyrrolyl propenoic acids **27–30**, which were in turn converted into the related hydroxamates by the previously described three-step procedure [29] – (i) formation of mixed anhydride with ethyl chloroformate; (ii) reaction with *O*-(2-methoxy-2-propyl)hydroxylamine [33]; and (iii) acidic treatment in the presence of Amberlyst® 15 (Scheme 1). Chemical and physical data of compounds **22–25**, **27–30** are listed in Table 2.

3. Results and discussion

3.1. Biology

In addition to compounds **1–21** [29], four (aryloxopropenyl)pyrrolyl hydroxamides (**22–25**) bearing some heteroaryl moieties at the oxopropenyl chain have been synthesized and tested against maize HD1-B and HD1-A, two homologues of mammalian class I and class II HDACs, respectively. As recently observed [29], the introduction of a variety of

Table 1
HD1-B and HD1-A inhibitory activity of compounds **1**–**25**[a]

Compound[b]	R	R_1	$IC_{50} \pm SD$ (μM)		Fold selectivity	
			HD1-B	HD1-A	Class I	Class II
1	Ph	H	0.26 ± 0.02	0.19 ± 0.01		
2	2-Cl–Ph	H	1.6 ± 0.08	0.05 ± 0.003		32.0
3	3-Cl–Ph	H	31.4 ± 1.26	0.44 ± 0.02		71.4
4	4-Cl–Ph	H	29.4 ± 1.18	18.6 ± 1.12		
5	2-F–Ph	H	3.4 ± 0.14	0.10 ± 0.004		34.0
6	3-F–Ph	H	38.8 ± 1.16	0.22 ± 0.01		176.4
7	4-F–Ph	H	24.9 ± 1.24	15.7 ± 0.94		1.6
8	2-Br–Ph	H	0.18 ± 0.007	0.21 ± 0.008		
9	3-Br–Ph	H	0.48 ± 0.04	1.6 ± 0.06	3.3	
10	4-Br–Ph	H	24.3 ± 0.97	20.3 ± 0.81		1.2
11	2-Me–Ph	H	0.39 ± 0.02	0.06 ± 0.002		6.5
12	3-Me–Ph	H	2.5 ± 0.08	0.17 ± 0.007		14.7
13	4-Me–Ph	H	4.8 ± 0.29	0.50 ± 0.02		9.6
14	2-MeO–Ph	H	0.17 ± 0.008	0.16 ± 0.01		
15	3-MeO–Ph	H	0.60 ± 0.03	0.39 ± 0.02		1.5
16	4-MeO–Ph	H	0.80 ± 0.05	0.79 ± 0.02		
17	1-Naphthyl	H	0.33 ± 0.02	0.01 ± 0.0007		33.0
18	2-Naphthyl	H	1.8 ± 0.07	0.04 ± 0.002		45.0
19	4-Biphenyl	H	31.8 ± 1.27	2.2 ± 0.07		14.4
20	Ph	Me	0.57 ± 0.02	0.78 ± 0.02	1.4	
21	Ph	Et	4.5 ± 0.22	0.22 ± 0.01		20.4
22	2-Thienyl	H	25.8 ± 1.55	16.3 ± 0.99		1.6
23	3-Thienyl	H	22.6 ± 0.90	13.8 ± 0.41		1.6
24	2-Furyl	H	19.7 ± 0.79	1.2 ± 0.06		16.4
25	5-DBF[c]	H	6.4 ± 0.32	2.1 ± 0.11		3.0
TSA			0.0004 ± 0.00001	0.0008 ± 0.00003	2.0	
SAHA			0.03 ± 0.001	0.18 ± 0.009	6.0	

[a] Data represent mean values of at least three separate experiments.
[b] Chemical and physical properties and inhibitory data for compounds **1**–**21** were described in Part 1.
[c] 5-DBF, 2,3-dihydrobenzofuran-5-yl.

substituents at the benzene C_2 or C_3 position of unsubstituted **1** gave an increase (C_2-substituted) or was well tolerated (C_3-substituted) for the HD1-A inhibitory activity. In particular, since the C_3-chloro and C_3-fluoro substituted compounds **3** and **6** showed little activity against HD1-B, they displayed the highest class II selectivity (selectivity ratio: 71.4 (**3**) and 176.4 (**6**)). The replacement of the benzene ring with the bulkier 1- and 2-naphthyl moieties (**17**, **18**) furnished highly active derivatives against HD1-A, although less selective than **3** and **6**.

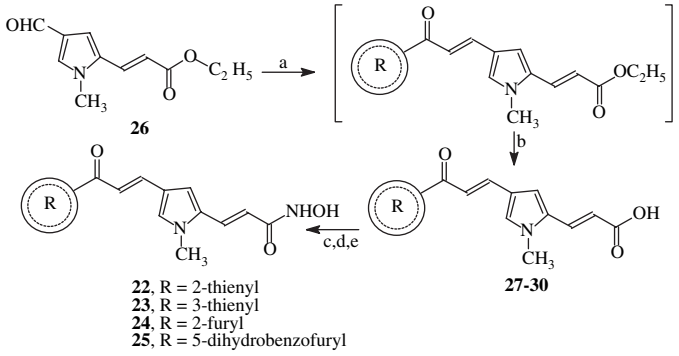

Scheme 1. Reagents and conditions: (a) Heteroaryl-methyl-ketone, C_2H_5ONa, C_2H_5OH, room temp. (b) KOH, C_2H_5OH, H_2O, room temp. (c) $ClCOOC_2H_5$, $(C_2H_5)_3N$, THF, 0 °C. (d) $NH_2OC(CH_3)_2OCH_3$. (e) Amberlyst® 15, MeOH, 45 °C.

Differently, when the benzene ring of **1** was replaced with heteroaryl groups such as 2- and 3-thienyl, 2-furyl, and 5-dihydrobenzofuryl a drop in the HD1-A inhibitory activity was observed, which is dramatic (86- and 73-fold) with the thiophene derivatives **22** and **23**, and less evident (6- and 11-fold) with the (benzo)furane-containing **24** and **25**. From these data, the most interesting (heteroaryloxopropenyl)pyrrolyl derivative was the 2-furyl-substituted **24**, which was scarcely active against HD1-B ($IC_{50} = 19.7$ μM) but showed low micromolar activity ($IC_{50} = 1.2$ μM) against HD1-A, thus reaching a selectivity ratio of 16.4.

On the reported (aryloxopropenyl)pyrrolyl hydroxyamides **1**–**25**, a number of 3-D QSAR studies has been performed with the aim to elucidate their activity and/or selectivity on HD1-B or HD1-A enzymes.

3.2. Molecular modelling studies

The molecular modelling studies can be divided into four sections:

(1) Training set and test set conformational search by simulated annealing in continuum solvent simulation (GBSA).
(2) Generation of 3-D QSAR models for HD1-A and HD1-B activities, using 3-D GRIND descriptors.

Table 2
Chemical and physical data for compounds **22–25**, **27–30**

Compound	R	R_1	Mp (°C)	Recrystn solvent	% Yield	Formula	Anal[a]
22	2-Thienyl	H	230–232	CH_3CN/MeOH	59	$C_{15}H_{14}N_2O_3S$	C, H, N, S
23	3-Thienyl	H	237–239	CH_3CN/MeOH	60	$C_{15}H_{14}N_2O_3S$	C, H, N, S
24	2-Furyl	H	235–237	CH_3CN/MeOH	58	$C_{15}H_{14}N_2O_4$	C, H, N
25	5-DBF[b]	H	242–244	MeOH	57	$C_{19}H_{18}N_2O_4$	C, H, N
27	2-Thienyl	H	250–252	CH_3CN/MeOH	73	$C_{15}H_{13}NO_3S$	C, H, N, S
28	3-Thienyl	H	226–228	CH_3CN/MeOH	76	$C_{15}H_{13}NO_3S$	C, H, N, S
29	2-Furyl	H	250–252	CH_3CN/MeOH	74	$C_{15}H_{13}NO_4$	C, H, N
30	5-DBF[b]	H	220–222	CH_3CN	69	$C_{19}H_{17}NO_4$	C, H, N

[a] Analytical results were within ±0.4% of the theoretical values.
[b] 5-DBF, 2,3-dihydrobenzofuran-5-yl.

(3) Homology modelling of the HD1-A and HD1-B enzymes.
(4) Docking of **6** and **9** compounds into HD1-A and HD1-B models.

3.2.1. Simulated annealing studies

Three-dimensional structures of compounds **1–25** were generated using the crystal structures of TSA and SAHA as templates. The resulting starting conformations were subjected to a simulated annealing procedure in continuum solvent simulation (GBSA), employing the MMFF94 force field (see Section 5 for details).

Analysis of the resulting minima conformations related to the (aryloxopropenyl)pyrrolyl hydroxamates **1–25** divides the training set molecules in straight shaped conformations (**8**, **9**, **14**, **15**, **20**, **22–25**; an example, Fig. 2B) and bow-shaped conformations (**1–7**, **10–13**, **16–19** and **21**; an example, Fig. 2A). A deeper inspection of the above conformations revealed that dihedral angle Φ (Fig. 1) could be considered a further structural feature influencing the HD1-B or HD1-A inhibitory activity. Indeed, from plots in Fig. 3 and data in Table A (Supplementary data) the highest absolute values of the Φ dihedral angles are associated with the most potent derivatives.

3.2.2. 3-D QSAR studies

The minimized structures were then imported in Almond (MIA, Perugia, Italy) to generate the GRIND descriptors in a three-step process (see details in Section 5). The GRIND descriptors obtained, 430 for HD1-B and 290 for HD1-A and correlated with the anti-HD1-B or anti-HD1-A activities (pIC_{50}s) and PLS models were generated and optimized by means of an iterative fractional factorial design (FFD) variable selection procedure while using five random group for the cross-validations.

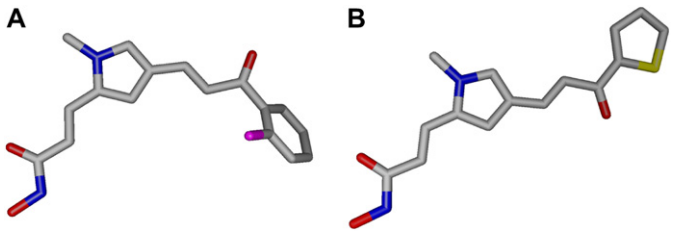

Fig. 2. (A) Example of folded-shaped molecule (**2**). (B) Example of straight shaped molecule (**22**).

3.2.2.1. HD1-B model. The best model for the (aryloxopropenyl)pyrrolyl hydroxamates **1–25** was obtained using the preliminary model number 48 (Table B in Supplementary data), characterized by the following settings: 150 filtered nodes, 75% of field weight, 0.8 smoothing window and 75% of the autocorrelogram size. A series of sequential fractional factorial design (FFD) selections allowed the definition of a final model with 223 descriptive variables and r^2 and q^2 values of 0.97 and 0.81, respectively (Fig. 4). Analogue FFD selections on the other 80 preliminary models listed in Table B (Supplementary data) could not afford any better model.

From the PLS scores plot generated by the GRIND descriptors (see Fig. A in Supplementary data), it was possible to notice a clear separation between the more and less differently active compounds. Thus, the model is suitable for the discrimination of highly active derivatives from poorly active ones. The PLS coefficient histogram shows the most important pairs of nodes that contribute negatively or positively to the anti-HD1-B activity (Fig. 5).

All 10 correlograms are reported sequentially with different colors: each bar height represents the variable PLS coefficient and a higher value corresponds to more significance of activity. The analysis of all the distances at higher PLS coefficients showed that DRY–N1: 6 and TIP–TIP: 27 variables are the most important to explain the 3-D structure–activity relationships for the HD1-B inhibition.

The DRY-N1: Six distance has the most favourable influence on the activity. This is a short distance (2.4 Å) between the C=O and the aromatic groups of the cap: this length is absent in all the molecules in which the two groups are co-planar inferring that for either HD1-B or HD1-A inhibitory activity some distortion of the Φ angle is necessary. As a matter of fact, the more active derivatives display higher dihedral angle Φ absolute values that correspond to higher nodes energy products (Fig. B in Supplementary data).

Contrary to all the above described distances, the TIP–TIP: 27 variable correlates negatively with the activity. It describes the length (10.8 Å) of the molecules being generated by hydroxamic acid and the cap shape fields, and it is present only in two of the lowest active compounds, **6** (Fig. 6) and

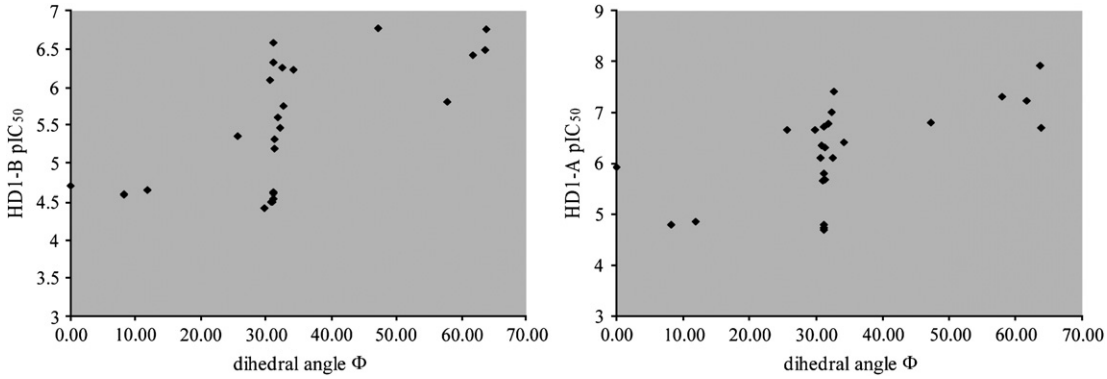

Fig. 3. Plots of inhibitory potency (left: HD1-B; right: HD1-A) as a function of Φ dihedral angle.

3, bearing a fluorine and chorine atoms at the benzene-C_3 position, respectively. Interestingly, the same compounds are also the most selective against the HD1-A enzyme.

3.2.2.2. HD1-A model. The best model for the (aryloxopropenyl)pyrrolyl hydroxamates **1**–**25** was obtained using the preliminary model number 12 (Table C in Supplementary data), characterized by the following settings: 100 filtered nodes, 75% of field weight, 0.8 smoothing window and 50% of the autocorrelogram size. A series of sequential fractional factorial design (FFD) selections allowed the definition of the final model with 181 descriptive variables and r^2 and q^2 values of 0.98 and 0.85, respectively (Fig. 7). Analogue FFD selections on the other 80 preliminary models listed in Table C could not afford any better model.

From the PLS scores plot generated by the GRIND descriptors (Fig. C, Supplementary data), it was possible to notice a clear separation between the more and less active compounds. Thus, also this HD1-A model is effectively able to discriminate highly active derivatives from poorly active ones. The PLS coefficient histogram shows the most important pairs of nodes that contribute negatively or positively to the anti-HD1-A activity (Fig. 8).

The analysis of the distances at higher PLS coefficients showed that DRY–N1:7, O–TIP: 21 and DRY–O: 10 variables are the most important ones.

The seventh variables of the DRY–N1 cross-correlogram is that with the highest PLS coefficient, and represents (Fig. 6B) the distance (2.8 Å) between an H-bond acceptor (C=O) and a hydrophobic (DRY) region at the cap. This distance is present in almost all the molecules, and the most active derivatives have energy interaction products higher than those with lower activity (Fig. D in Supplementary data). A deeper inspection of this distance shows that at negative values of the dihedral angle Φ correspond to higher values of energy products. The introduction of substituents bigger than fluorine at the *ortho* position of the **1** benzene ring increases the absolute value of the Φ angle, although higher activities are observed only for compounds displaying values less than −40° (Table A, Supplementary data).

The second important distance (O–TIP: 21) is around 8.4 Å, running from an H-bond donator field (red cloud over the NH of hydroxamic acid in Fig. 6C) to a polyhedron situated around the cap group. The cap shape seems to correlate with the anti-HD1-A activity, indeed if *para* substituents are introduced in the aromatic moiety the shape changes and the above distance increases (from 8.4 to 11.6 Å), as a consequence a decrease of activity is observed. Moreover, molecules with a straight shape (*i.e.*, **22**) or with the cap group folding in an opposite direction of NH (*i.e.*, **21**) do not show this distance and have low activity.

Finally, a distance of about 4 Å between the NH group and the aromatic portion (DRY–O: 10, Fig. 6D) has also a high PLS *coefficient*, and it is present only in molecules with the highest anti-HD1-A activity (**2**, **11**, and **17**). While the previous distances (DRY–N1: 7 and O–TIP: 21) gave insights in

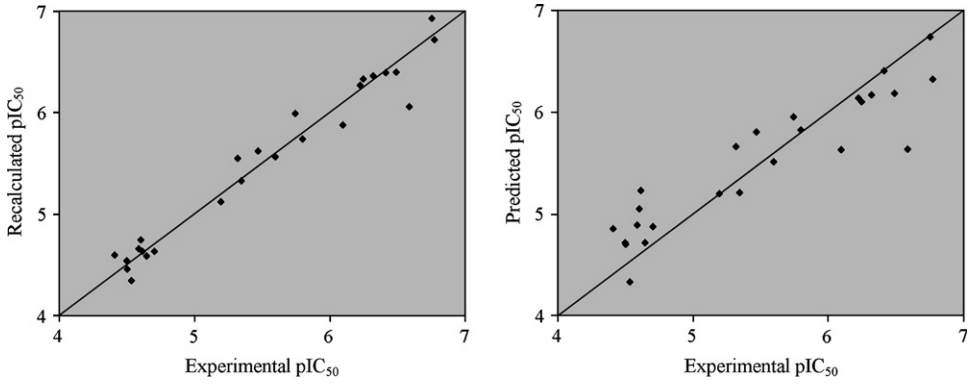

Fig. 4. Left: fitting plot between the experimental and the calculated pIC$_{50}$. Right: cross-validation plot between the experimental and the predicted pIC$_{50}$ (four principal components).

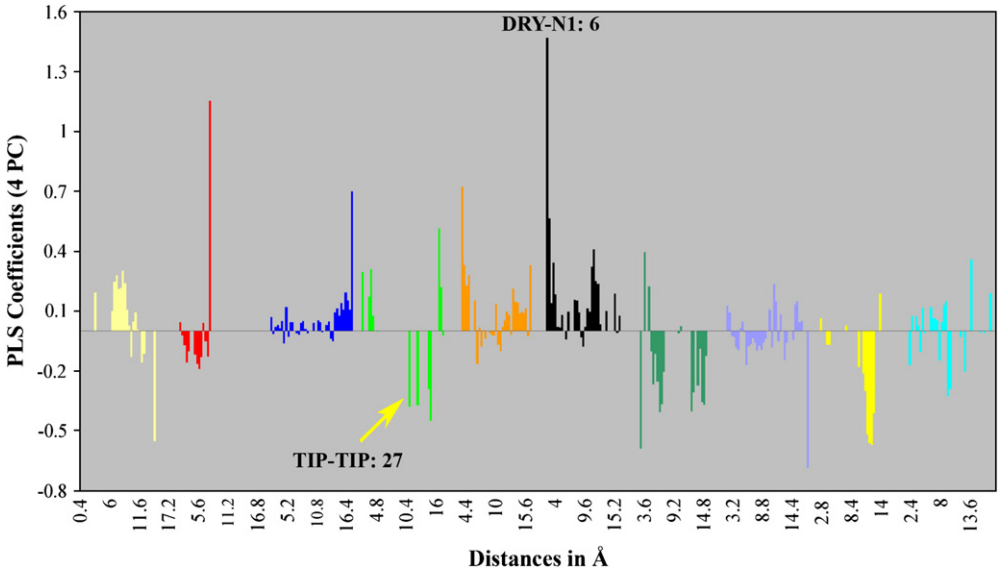

Fig. 5. HD1-B PLS coefficients plot. GRIND variable DRY–N1-6 has a strong positive correlation to the biological activity (Y) while the TIP–TIP-27 has a negative correlation. Correlogram description: light yellow: DRY–DRY, red: O–O, blue: N1–N1, green: TIP–TIP, orange: DRY–O, black: DRY–N1, dark green: DRY–TIP, violet: O–N1, yellow: O–TIP, magenta: N1–TIP. The PLS coefficient are plotted *vs* the distances between two MIF nodes (For interpretation of the references to colour in the figure legends, the reader is refered to the web version of this article.).

discriminating highly active compounds from low active ones, the presence of the DRY–O: 10 distance is a direct indicator of very high active derivatives, being the consequence of the contemporary presence of the DRY–N1: 7 and O–TIP: 21 descriptors. In fact the most active derivatives are bow-shaped and all have *ortho* substituents greater than fluorine (chlorine for **2**, methyl for **11**, and C2, C3-fused phenyl for **17**) at the benzene unit, and have Φ values less than −40°.

3.2.3. Selectivity predictions

To test the validity of the above described models, a test set was compiled with 14 unpublished (aryloxopropenyl)pyrrolyl hydroxyamides analogues (Table 3) and the HD1-B and HD1-A inhibitory activities were predicted (Table 4). As can be seen from data in Table 4, the application of the two models effectively recognized derivatives **31–44** to be all selective against class II HDAC. Interestingly, all the derivatives

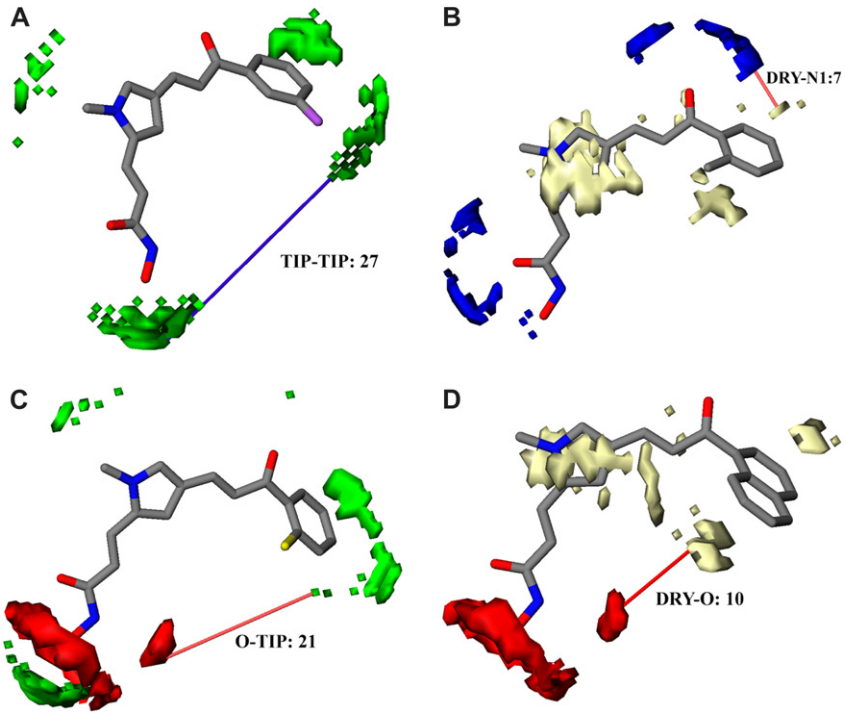

Fig. 6. TIP–TIP-27 distance for compound **6**. (B) Distance between a H-acceptor bond group and a hydrophobic one in **11**, represented in the PLS coefficient plot as DRY–N1: 7th variable (the most intensive interaction). If the aromatic portion is co-planar to the C=O, the distance is not present. (C) Interaction present in **2** between the H-acceptor bond group and the capping shape (O–TIP-21). (D) DRY–O-10 distance in **17**.

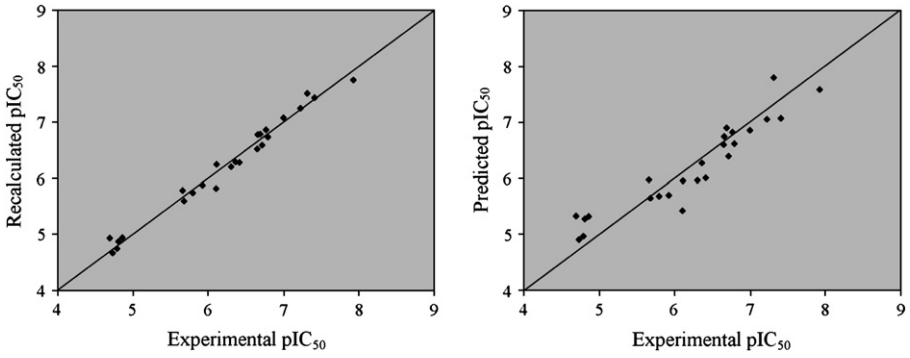

Fig. 7. Left: fitting plot of the experimental pIC_{50} against the calculated one. Right: cross-validation plot between the experimental pIC_{50} and the predicted one (four principal components).

included in the test set displayed an overall tendency to adopt straight SA conformations (Fig. E, Supplementary data), in agreement with the above observations.

3.2.4. Homology modelling and docking studies

Using the CPH models 2.0 Server [34], homology models for HD1-A [27] and HD1-B [25] sequences were derived employing the structural data of the HDAC8/TSA complex [35] filed in the Brookheaven database [36] (PDB entry code 1t64). The models were refined using a molecular dynamics (MD) protocol (see Section 5) by means of the program AMBER 8 [37]. HD1-B homology model was compared to HDAC8 X-ray structure, while HD1-A homology model to that of HDAH (PDB entry code 1zz1). They showed a similar 3-D structures especially around the catalytic sites (Figs. F and G, Supplementary data) thus supporting the obtained homology models.

Comparing the MD average structures of the HD1-A and HD1-B homology models, the most striking difference between the two enzymes resides in three loops (sequences 49–73, 173–199 and 277–283 for HD1-A; 50–74, 169–190 and 267–273 for HD1-B), two of which (HD1-$A_{49–73}$/HD1-$A_{173–199}$ and HD1-$B_{50–74}$/HD1-$B_{169–190}$) form the entrance of the channel that leads to the catalytic zinc ion, and one (HD1-$A_{277–283}$, HD1-$B_{267–273}$) is close to the end of channel near the catalytic zone. These three loops show a different conformation and spatial disposition (Fig. H in Supplementary data) that could account for possible different substrate specificity. In particular, in the proximity of the TSA cap group (dimethylaminobenzene) (see Fig. I in Supplementary data) the two enzymes show opposite side-chain charged residues: in HD1-B the negative Glu67–γCOO group points towards the catalytic site entrance reducing the volume cavity while in HD1-A the positive Lys59–ϵ-NH_3^+ group is

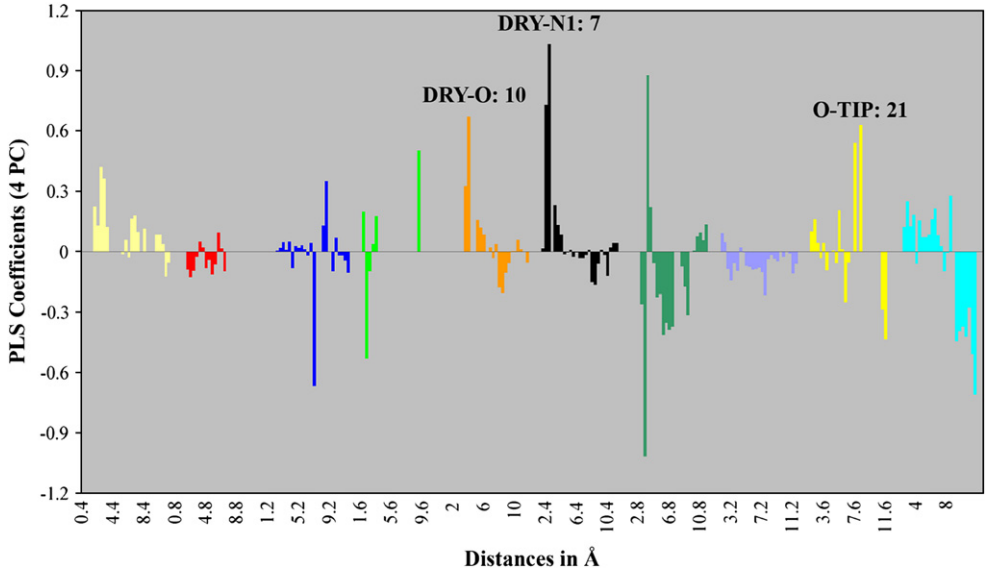

Fig. 8. PLS coefficient histogram showing the importance of single descriptors to explain the $pIC_{50}(Y)$: positive values of a coefficient indicate a direct correlation to the Y, and negative ones indicate an inverse correlation to the Y. Correspondingly, GRIND variables DRY–O: 10, DRY–N1: 7 and O–TIP: 21 have a strong positive correlation to the biological activity (Y). DRY–N1: 7 represents the variable number 7 obtained between the fields generated by the hydrophobic and amide probes. Correlogram description: light yellow: DRY–DRY, red: O–O, blue: N1–N1, green: TIP–TIP, orange: DRY–O, pink: DRY–N1, light green: DRY–TIP, violet: O–N1, yellow: O–TIP, light blue: N1–TIP. The PLS coefficient are plotted *vs* the distances between two MIF nodes. (For interpretation of the references to colour in the figure legends, the reader is refered to the web version of this article.).

Table 3
Structures and experimental activities of **31–44**[a]

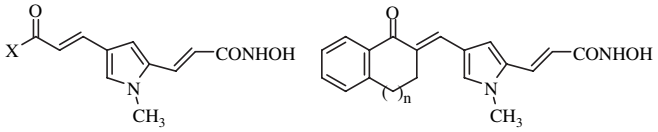

31-40,43,44 **41** (n=1), **42** (n=2)

Compound	X	$IC_{50} \pm SD$ (μM)		Class selectivity
		HD1-B	HD1-A	Class I/Class II
31	2,3-Cl_2–Ph	17.2 ± 0.86	6.8 ± 0.27	2.5
32	2,5-F_2–Ph	16.6 ± 0.83	0.80 ± 0.04	20.8
33	3,4-F_2–Ph	13.5 ± 0.41	2.2 ± 0.11	6.1
34	3,4-Cl_2–Ph	21.3 ± 0.85	5.9 ± 0.24	3.6
35	3,5-F_2–Ph	23.5 ± 1.18	2.1 ± 0.08	11.2
36	2,4-Cl_2–Ph	17.0 ± 0.68	2.8 ± 0.11	6.1
37	2,6-F_2–Ph	0.807 ± 0.02	0.167 ± 0.01	4.8
38	3-Cl-4-F–Ph	1.4 ± 0.06	0.50 ± 0.03	2.8
39	2-Benzofuranyl	12.0 ± 0.36	3.0 ± 0.15	4.0
40	1,4-Benzo dioxan-6-yl	0.621 ± 0.23	0.185 ± 0.007	3.4
41		59.0 ± 2.36	3.4 ± 0.14	17.3
42		0.51 ± 0.02	0.196 ± 0.008	2.6
43	3-CF_3–Ph	159.0 ± 6.4	9.3 ± 0.46	17.1
44	3-CF_3O–Ph	298.0 ± 14.9	90.0 ± 4.5	3.3

[a] The synthesis of compounds **31–42** will be reported elsewhere. Compounds **43** and **44** were reported in Ref. [27].

faraway from the rim cavity making and a wider entrance results. Close to the enantiomeric TSA C6-methyl group in HD1-A there is a Phe–Tyr sequence (Phe179–Tyr180), which is inverted in HD1-B (Tyr172–Phe173).

The $Tyr172_{HD1\text{-}B}$ phenolic group seems to narrow the catalytic channel by the means of a hydrogen bond with the backbone carbonyl group of Leu239, forming a hydrophobic pocket that hosts the TSA C6-methyl group. On the other hand, the inverted sequence in HD1-A does not allow the hydrogen bond formation, and no pocket is shown. Finally the last major difference is in the channel well depth: HD1-B shows a smaller acetyl escape channel [38] compared to that of HD1-A, due to a hydrogen bond formation between $His108_{HD1\text{-}B}$ and $Gly268_{HD1\text{-}B}$ (distance $\varepsilon\text{-}N_{His108} \cdots O{=}C_{Gly268} = 2.96$ Å).

Using the Autodock [39] program the MD average structures of the HD1-A and HD1-B homology models allowed to further investigate in the putative binding mode of either **9** (HD1-B most selective derivative) or **6** (HD1-A most selective compound). A direct comparison of the **9**/HD1-B and **6**/HD1-A binding modes are quite different, thus reflecting the above reported structural dissimilarities between HD1-B and HD1-A models.

Inspection of the **9**/HD1-B complex shows a tight Zn^{+2} chelation as the **9** hydroxamic carbonyl oxygen is at a distance of only 1.70 Å from the ion; moreover the aroyl carbonyl oxygen is at a hydrogen bonding distance to the Tyr172 hydroxyl (2.84 Å) and a favourable π–π interaction exists between the **9** pyrrole and Phe173 phenyl rings (Fig. L in Supplementary data). Similarly as observed in the **9**/HD1-B complex, the HD1-A **6** bound conformation seems to efficiently bind the Zn^{+2} ion ($C{=}O \cdots Zn^{+2}$ distance = 1.97 Å; $OH \cdots Zn^{+2}$ distance = 2.57 Å). Furthermore, **6** makes at least three other favourable interactions: a weak hydrogen bond between the **6** aroyl carbonyl oxygen and the Asn58 side-chain NH (distance 3.54 Å), a hydrogen bond between the **6** fluorine atom and the Gly117 backbone NH (distance 2.6 Å) and π–π interaction between the pyrrole and Phe118 aromatic rings (Fig. L, Supplementary data). One can argue that such distances are not in agreement with the experimental X-ray structures reported for either SAHA or TSA. Nevertheless, among the 100 Autodock conformations some of them displayed more efficiently Zn chelating distances (not shown). In this paper we focused on the Autodock best scored poses. Interestingly, the **6** and **9** SA generated conformations are in good agreement with Autodock proposed **6**/HD1-A and **9**/HD1-B bound conformations (Fig. M in Supplementary data); moreover, the computed distances between the halogen atoms (fluorine in **6** and bromine in **9**) and the hydroxamic nitrogen are comparable to those above highlighted from the 3-D QSAR analysis (Fig. 9, and Fig. N in Supplementary data).

Table 4
Test set prediction of HD1-B and HD1-A pIC_{50}s

Compound	Actual pIC_{50}		Pred. pIC_{50}		Pred. class II selectivity
	HD1-B	HD1-A	HD1-B	HD1-A	
31	4.765	5.168	6.243	8.009	58.3
32	4.780	6.097	5.144	6.426	19.2
33	4.870	5.658	4.449	6.670	166.2
34	4.672	5.229	4.736	6.499	58.0
35	4.629	5.678	4.725	7.127	252.5
36	4.921	5.523	4.727	5.173	2.8
37	4.770	5.553	4.938	5.756	6.6
38	6.207	6.733	5.365	6.452	12.2
39	4.229	5.469	4.790	5.669	7.6
40	6.292	6.708	5.949	6.856	8.1
41	6.093	6.777	5.721	6.509	6.1
42	5.854	6.301	5.398	6.368	9.3
43	3.799	5.032	4.974	7.176	159.3
44	3.526	4.046	5.545	6.831	19.3

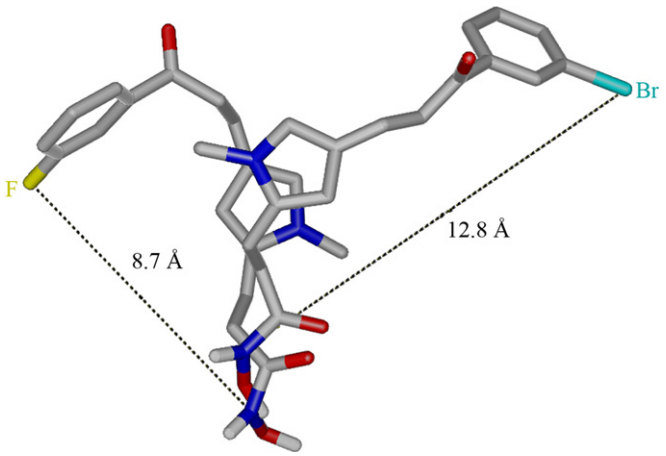

Fig. 9. Docked conformation of **6** (fluorine atom in yellow) and **9** (bromine atom in cyan). (For interpretation of the references to colour in the figure legends, the reader is refered to the web version of this article.).

4. Conclusions

Because class II HDACs selective inhibitors may have great potential as biological tools to elucidate some still unknown class II HDAC functions, in this paper we have reported alignment-independent 3-D QSAR studies on a series of 25 (aryloxopropenyl)pyrrolyl hydroxamides active against both HD1-B (homologous of class I HDACs) and HD1-A (homologous of class II HDACs) enzymes.

Comparing the two PLS coefficients plots it was possible to put in evidence some similarities and differences between the models. Both plots showed the most important variable to be the distance between an H-acceptor bond group (C=O) and an aromatic portion of the cap (DRY–N1: 6 for HD1-B and DRY–N1: 7 for HD1-A). This distance was present only if the C=O and the aromatic portion were not planar, meaning that the Φ torsional angle is a fundamental requirement for both activities. The differences were evident especially in the O–TIP and TIP–TIP correlograms, suggesting that a bended molecular shape is important for a selective HD1-A activity, while a straight molecular shape is important for HD1-B activity. To validate the two 3-D QSAR models a test set of 14 compounds not used to define the models themselves were used. The two models correctly predicted that all the derivatives in the test set were selective against class II HDAC. Moreover, all the test set conformations turned out to be straight shaped. Docking studies of the HD1-A and HD1-B most selective derivatives **6** and **9** confirmed the geometrical requisite for the APHA class I/class II selectivity.

In conclusion, the reported 3-D QSAR models helped the interpretation of the selectivity issue for the class I and II HDAC inhibitors, although for class I selectivity some uncertainty is still present due to the fact that at the moment no highly HD1-B-selective aryloxopropenylpyrrolyl hydroxyamides have yet been disclosed. Further synthetic and molecular modelling efforts are in progress to fill this gap.

5. Experimental protocols

5.1. Chemistry

Melting points were determined on a Büchi 530 melting point apparatus and are uncorrected. Infrared (IR) spectra (KBr) were recorded on a Perkin–Elmer Spectrum One instrument. ^{1}H NMR spectra were recorded at 200 MHz on a Bruker AC 200 spectrometer; chemical shifts are reported in δ (ppm) units relative to the internal reference tetramethylsilane (Me_4Si). All compounds were routinely checked by TLC and ^{1}H NMR. TLC was performed on aluminum-backed silica gel plates (Merck DC-Alufolien Kieselgel 60 F_{254}) with spots visualized by UV light. All solvents were reagent grade and, when necessary, were purified and dried by standards methods. Concentration of solutions after reactions and extractions involved the use of a rotary evaporator operating at a reduced pressure of *ca*. 20 Torr. Organic solutions were dried over anhydrous sodium sulfate. Analytical results are within ±0.40% of the theoretical values. A SAHA sample for biological assays was prepared as previously reported by us [40]. All chemicals were purchased from Aldrich Chimica, Milan (Italy) or Lancaster Synthesis GmbH, Milan (Italy) and were of the highest available purity.

5.1.1. General procedure for the synthesis of 3-[4-(3-heteroaryl-3-oxopropen-1-yl)-1-methyl-1H-pyrrol-2-yl]-2-propenoic acids **27–30** – example: 3-[4-(3-(2-furyl)-3-oxo-1-propen-1-yl)-1-methyl-1H-pyrrol-2-yl]-2-propenoic acid **29**

Sodium metal (0.60 g, 26.2 mmol) was dissolved in 50 mL of absolute ethanol, and ethyl 3-(4-formyl-1-methyl-1*H*-pyrrol-2-yl)-2-propenoate **26** (4.8 mmol, 1.00 g) and 2-acetylfurane (4.8 mmol, 0.53 g) were added to the clear solution. The mixture was stirred at room temperature for 3 h, then it was treated with 2 N KOH (19.2 mmol, 1.07 g), and the resulting mixture was stirred at room temperature for further 3 h. Afterward, the solution was poured into water (200 mL) and was made acidic with 2 N HCl. The obtained precipitate was filtered and recrystallized to give the pure acid **29**. ^{1}H NMR (DMSO-d_6) δ 3.74 (s, 3H, NCH_3), 6.34 (d, 1H, CH=C*H*COOH), 6.75 (m, 1H, furane H-4), 6.95 (d, 1H, pyrrole β-proton), 7.13 (d, 1H, pyrrole α-proton), 7.46 (d, 1H, COC*H*=CH), 7.56 (d, 1H, COCH=C*H*), 7.70 (m, 2H, C*H*=CHCOOH and furane H-3), 8.01 (d, 1H, furane H-5), 12.22 (s, 1H, OH). Anal. ($C_{15}H_{13}NO_4$) C, H, N.

5.1.2. General procedure for the synthesis of 3-[4-(3-heteroaryl-3-oxopropen-1-yl)-1-methyl-1H-pyrrol-2-yl]-n-hydroxy-2-propenamides **22–25** – example: 3-[4-(3-(2-thienyl)-3-oxo-1-propen-1-yl)-1-methyl-1H-pyrrol-2-yl]-N-hydroxy-2-propenamide **22**

Ethyl chloroformate (5.6 mmol, 0.6 mL) and triethylamine (6.0 mmol, 0.9 mL) were added to a cooled (0 °C) solution of 3-[4-(3-(2-thienyl)-3-oxopropen-1-yl)-1-methyl-1*H*-pyrrol-2-yl]-2-propenoic acid **27** (4.7 mmol, 1.34 g) in dry THF (10 mL), and the mixture was stirred for 10 min. The solid was filtered off, and *O*-(2-methoxy-2-propyl)hydroxylamine (14.1 mmol, 1.3 mL) [40] was added to the filtrate. The solution was stirred for 15 min at 0 °C, then it was evaporated under reduced pressure, and the residue was diluted in methanol (30 mL). Amberlyst® 15 ion-exchange resin (0.6 g) was added to the solution of the *O*-protected hydroxamate, and the mixture was stirred at 45 °C for 1 h. Afterward, the reaction was filtered and the filtrate was concentrated in vacuo to give the crude **22**, which was purified by crystallization. ^{1}H NMR (DMSO-d_6) δ 3.74 (s, 3H, NCH_3), 6.33 (d, 1H, CH=C*H*–CONHOH), 6.70 (m, 1H, pyrrole β-proton), 7.17 (m, 1H, pyrrole α-proton), 7.27 (s, 1H, thiophene H-4), 7.45 (d, 1H, C*H*=CH–CONHOH), 7.60 (d, 1H, COC*H*=CH), 7.71 (d, 1H, COCH=C*H*), 7.99 (d, 1H, thiophene H-3), 8.20 (m, 1H, thiophene H-5), 9.00 (s, 1H, NH exchangeable with D_2O), 10.69 (s, 1H, OH exchangeable with D_2O). Anal. ($C_{15}H_{14}N_2O_3S$) C, H, N, S.

5.2. Biology

5.2.1. In vitro maize HD1-B and HD1-A inhibition

Radioactively labeled chicken core histones were used as the enzyme substrate according to established procedures [41–43]. The enzyme liberated tritiated acetic acid from the substrate, which was quantified by scintillation counting. IC_{50} values are results of triple determinations. A 50 μL sample of maize enzyme (at 30 °C) was incubated (30 min) with 10 μL of total [^{3}H]acetate-prelabeled chicken reticulocyte histones (2 mg/mL). Reaction was stopped by addition of 50 μL of 1 M HCl/0.4 M acetate and 800 μL of ethyl acetate. After centrifugation (10 000 g, 5 min), an aliquot of 600 μL of the upper phase was counted for radioactivity in 3 mL of liquid scintillation cocktail. The compounds were tested at a starting concentration of 40 μM, and active substances were diluted further. TSA and SAHA were used as the reference compounds, and blank solvents were used as negative controls.

5.3. Molecular modelling

5.3.1. 3-D QSAR, homology modelling and docking studies

Molecular modelling analyses were performed using the software packages Macromodel 7.1 [44], graphical interface Maestro 3.0 and Almond 3.2.0a [30] running on IBM compatible AMD Athlon 3.0 GHz workstations with the linux operating system SUSE 9.0 distribution.

(Aryloxopropenyl)pyrrolyl hydroxyamides **1–25** (Table 1) were modelled using the Maestro program using as a template the crystal structures of TSA or SAHA extracted from the HDLP/TSA or HDLP/SAHA complexes [36,45–47], respectively (pdb entry codes: 1c3r for TSA/HDLP and 1c3s for SAHA/HDLP).

The training set or test set starting conformations were obtained using a MD protocol using a simulated annealing procedure as implemented in Macromodel version 7.1and it was conducted as follows: each complex was energy minimized to a low gradient. The non-bonded cut-off distances were set to 20 Å for both van der Waals and electrostatic interactions. An initial random velocity to all atoms corresponding to 300 K was applied. Three subsequent molecular dynamics runs were then performed. The first was carried out for 10 ps with a 1.5 fs time-step at a constant temperature of 300 K for equilibration purposes. The next molecular dynamic was carried out for 20 ps, during which the system is coupled to a 150° thermal bath with a time constant of 5 ps. The time constant represents approximately the half-life for equilibration with the bath; consequently the second molecular dynamic command caused the molecule to slowly cool to approximately 150 K. The third and last dynamic cooled the molecule to 50 K over 20 ps. A final energy minimization was then carried out for 250 iterations using conjugate gradient. The minimizations and molecular dynamics were in all cases performed in simulated aqueous solution using the batchmin GBSA keyword and the MMFF94 force field.

The same MD procedure was also applied to the reference compounds TSA and SAHA. It could be argued that both the duration and temperature of the SA simulations would only allow crossing of very small barriers; therefore we repeated the SA simulation using different starting conformations using the PRODGR software. The SA performed on the PRODRG conformation were almost completely superimposable to those generated starting from the TSA/SAHA bound conformations.

The minimized structures were then imported in Almond (MIA, Perugia, Italy) to generate the GRIND descriptors in a three-step process: first, the molecular interaction fields (MIF) of the compounds were calculated by GRID using four chemical probes: DRY (hydrophobic), O (carbonyl), N1 (amide) and TIP (shape) [48] in order to present hydrophobic, H-bond acceptor, H-bond donor and steric interactions with a virtual receptor site (VRS); second, the MIF were filtered using a Federov-like algorithm procedure to select the points (nodes) with the lowest energy (most favourable interactions) and the greatest distance between them, and finally the filtered max interactions were plotted as energy *vs* distance in auto- and cross-correlograms [32,49]. These interaction energies at specified distances correspond to the GRIND descriptors [49]. Varying the Almond setting parameters (number of filtered nodes, % field weight, smoothing window and autocorrelograms size), 81 3-D QSAR models for each activity were built to evidence the best one to explain the relationship between structure–HD1-B/HD1-A activities of the 25 compounds (Tables B and C in the Supplementary data). The four probes were conserved for all the models because they could best represent the HD1-B and HD1-A protein binding sites [30]. The grid space was set to 0.5 Å, the smoothing window was changed from 0.8 to 2.0 grid units and the autocorrelogram size from 0 to 75%. The number of nodes was experimented from 100 to 200 and the relative weight of the field from 25 to 75% to see if the distances between the molecular interaction fields (MIFs) were more important than the energy products. The variables were grouped in blocks (correlograms) depending on which kind of favourable interaction (hydrophobic and hydrogen bonding) is represented for each one of the points. The GRIND descriptors obtained, 430 for HD1-B and 290 for HD1-A, were binned into 10 correlograms: four autocorrelograms (DRY–DRY, O–O, N1–N1 and TIP–TIP) and six cross-correlograms (DRY–O, DRY–N1, DRY–TIP, O–N1, O–TIP and N1–TIP). The anti-HD1-B or anti-HD1-A activity was imported into Almond as pIC_{50} ($-\log_{10}(IC_{50})$) and PLS models were generated and cross-validated. To optimize the PLS models an iterative fractional factorial design (FFD) variable selection procedure was applied. The effect of dummy variables (20%) on the predictivity was calculated and only if a variable had a positive effect on the predictivity larger than the effect of the average dummy variable the variable was included in the final model. The FFD selection was repeated until the r^2 and q^2 value did not increase significantly. In the FFD selection the cross-validation was conducted using five random groups for 20 times and a maximum of five principal components and retaining the uncertain variables. The models were validated using random groups. Molecules were assigned in a random way to five groups of equal size. Reduced models were built keeping

out one group at a time. The formation of the groups was repeated 20 times and using a maximum model dimensionality of three components.

The class I (HD1-B) and class II (HD1-A) HDAC homologues structures were prepared using the respective sequence deposited in the TrEMBL Protein Database (entry codes P56521 for HD1-B and Q7XAX9 for HD1-A). The homology models were automatically obtained by feeding the CPHmodels 2.0 Server [34] with the above sequences and using the HDAC8/TSA complex as template (pdb entry code 1t64) (Figs. O and P in Supplementary data). The two models were then refined by the AMBER 8.0 program using the following protocol. Firstly, the experimental bound conformation of TSA as found in the template was merged into either HD1-A or HD1-B complexes. AM1-BCC charges were calculated on the TSA (after the addition of the hydrogen atoms) employing the antechamber module of Amber 8.0. Using the xLeap AMBER module, the starting complexes were solvated in a octahedral box of Monte Carlo TIP3P water with each box side at least 10.0 Å away from the nearest atoms of the complexes. Sodium ions were included to neutralize the charge of the system. The ions were placed randomly (by replacing water molecules) in the system more than 10 Å away from each other and from the nearest atoms. The hydrogen atoms, counterions, and water molecules were then minimized for 1000 iterations. Then the whole complexes were relaxed for 5000 iterations. The MD simulations were performed with the smooth particle-mesh Ewald (PME) method employed to accommodate long-range electrostatic forces and with periodic boundary conditions at constant volume. The simulations utilized the Amber all-atom (parm99) and the GAFF force fields with a step size of 2 femtoseconds (fs). By using an extended list technique, the non-bonded interactions were effectively updated every step with a small overhead in computational cost. The non-bonded cut-off for van der Waals interactions was set to 10 Å. All covalent bonds involving hydrogen atoms were constrained using SHAKE. The ions and water molecules were then equilibrated for 20 ps at constant volume followed by energy minimization while freezing the model complex. Then a second equilibration was carried out for 90 ps while gradually unfreezing the bound TSA. A final equilibration of further 150 ps was carried out on the whole complexes without any restrain. During the equilibrations the stability of the complexes were monitored via their root mean square deviations (RMSD) (Figs. Q and R in Supplementary data). By means of the ptraj module the average structures were obtained from the last part of equilibrations and energy minimized for 1000 iterations as suggested in the AMBER manual and tutorials. Deletions of the bound TSA molecules lead to the HD1-A and HD1-B models used for the subsequent docking studies.

The docking studies were performed using Autodock 3.0.5. The Zn parameters included in the Autodock mkdpf program were used. Attempts to use other derived zinc parameters could not afford better results. The molecular structures of derivatives **6** and **9** were drawn using the PRODGR software which gave directly the molecule ready to be used by Autodock. The AutodockTools package was employed to generate the docking input files and to analyze the docking results, the same procedure as described in the manual was followed. All the non-polar hydrogens and the water molecules were removed. The Kollmann charges were loaded for the proteins while the charges applied by the PRODRG program [50] were retained in the ligand. A grid box size of $40 \times 40 \times 60$ points with a spacing of 0.375 Å between the grid points was implemented and covered most of the catalytic channel of either enzyme. The grid was centered on the mass center of the bound TSA. For all the inhibitors, the single bonds including the amide bonds were treated as active torsional bonds. One hundred structures, *i.e.*, 100 runs, were generated by using genetic algorithm searches. A default protocol was applied, with an initial population of 50 randomly placed individuals, a maximum number of 2.5×10^6 energy evaluations, and a maximum number of 2.7×10^4 generations. A mutation rate of 0.02 and a crossover rate of 0.8 were used. In a parallel docking experiment the bound TSA molecules extracted from either average MD equilibrated complexes were docked again. Autodock proved to reposition the TSA with a minimal RMSD error ($RMSD_{TSA\text{-}HD1\text{-}A} = 1.29$, $RMSD_{TSA\text{-}HD1\text{-}B} = 0.95$). Unfortunately the scores of the docked compound **6** and **9** were not comparable to the experimental. Autodock calculated either **6** or **9** to be nanomolar active derivatives, while they are only slightly below the micromolar range (see Table 1).

Acknowledgements

Many thanks are due to Prof. Gabriele Cruciani (Molecular Discovery, Perugia, Italy) for having kindly provided the ALMOND program. This work was supported by grants from PRIN 2004 and AIRC 2005.

Appendix. Supplementary data

Supplementary data associated with this article can be found in the online version at doi:10.1016/j.ejmech.2007.05.004

References

[1] B.D. Strahl, C.D. Allis, Nature 403 (2000) 41–45.
[2] F.D. Urnov, A.P. Wolffe, Emerg. Ther. Targets 4 (2000) 665–685.
[3] R.W. Johnstone, Nature Reviews Drug Discovery 1 (2002) 287–299.
[4] C.M. Grozinger, S.L. Schreiber, Chemistry and Biology 9 (2002) 3–16.
[5] A. Mai, S. Massa, D. Rotili, I. Cerbara, S. Valente, R. Pezzi, S. Simeoni, R. Ragno, Medicinal Research Reviews 25 (2005) 261–309.
[6] A. Lusser, G. Brosch, A. Loidl, H. Haas, P. Loidl, Science 277 (1997) 88–91.
[7] E. Verdin, F. Dequiedt, H.G. Kasler, Trends in Genetics 19 (2003) 286–293.
[8] G. Blander, L. Guarente, Annual Review of Biochemistry 73 (2004) 417–435.
[9] M.G. Guenther, M.A. Lazar, Methods in Enzymology 364 (2003) 246–257.
[10] A. Matsuyama, T. Shimazu, Y. Sumida, A. Saito, Y. Yoshimatsu, D. Seigneurin-Berny, H. Osada, Y. Komatsu, N. Nishino, S. Khochbin, S. Horinouchi, M. Yoshida, The EMBO Journal 21 (2002) 6820–6831.

[11] M. Gottlicher, S. Minucci, P. Zhu, O.H. Kramer, A. Schimpf, S. Giavara, J.P. Sleeman, F. Lo Coco, C. Nervi, P.G. Pelicci, T. Heinzel, The EMBO Journal 20 (2001) 6969–6978.
[12] R. Furumai, A. Matsuyama, N. Kobashi, K.H. Lee, M. Nishiyama, H. Nakajima, A. Tanaka, Y. Komatsu, N. Nishino, M. Yoshida, S. Horinouchi, Cancer Research 62 (2002) 4916–4921.
[13] A. Saito, T. Yamashita, Y. Mariko, Y. Nosaka, K. Tsuchiya, T. Ando, T. Suzuki, T. Tsuruo, O. Nakanishi, Proceedings of the National Academy of Sciences of the United States of America 96 (1999) 4592–4597.
[14] E. Hu, E. Dul, C.M. Sung, Z. Chen, R. Kirkpatrick, G.F. Zhang, K. Johanson, R. Liu, A. Lago, G. Hofmann, R. Macarron, M. de los Frailes, P. Perez, J. Krawiec, J. Winkler, M. Jaye, The Journal of Pharmacology and Experimental Therapeutics 307 (2003) 720–728.
[15] S.J. Haggarty, K.M. Koeller, J.C. Wong, C.M. Grozinger, S.L. Schreiber, Proceedings of the National Academy of Sciences of the United States of America 100 (2003) 4389–4394.
[16] T. Suzuki, A. Kouketsu, Y. Itoh, S. Hisakawa, S. Maeda, M. Yoshida, H. Nakagawa, N. Miyata, Journal of Medicinal Chemistry 49 (2006) 4809–4812.
[17] A.R. Guardiola, T.P. Yao, The Journal of Biological Chemistry 277 (2002) 3350–3356.
[18] A. Mai, S. Massa, R. Pezzi, D. Rotili, P. Loidl, G. Brosch, Journal of Medicinal Chemistry 46 (2003) 4826–4829.
[19] A. Mai, S. Massa, I. Cerbara, S. Valente, R. Ragno, P. Bottoni, R. Scatena, P. Loidl, G. Brosch, Journal of Medicinal Chemistry 47 (2004) 1098–1109.
[20] A. Mai, S. Massa, R. Ragno, I. Cerbara, F. Jesacher, P. Loidl, G. Brosch, Journal of Medicinal Chemistry 46 (2003) 512–524.
[21] A. Mai, S. Massa, R. Ragno, M. Esposito, G. Sbardella, G. Nocca, R. Scatena, F. Jesacher, P. Loidl, G. Brosch, Journal of Medicinal Chemistry 45 (2002) 1778–1784.
[22] S. Massa, A. Mai, G. Sbardella, M. Esposito, R. Ragno, P. Loidl, G. Brosch, Journal of Medicinal Chemistry 44 (2001) 2069–2072.
[23] R. Ragno, A. Mai, S. Massa, I. Cerbara, S. Valente, P. Bottoni, R. Scatena, F. Jesacher, P. Loidl, G. Brosch, Journal of Medicinal Chemistry 47 (2004) 1351–1359.
[24] D. Kolle, G. Brosch, T. Lechner, A. Pipal, W. Helliger, J. Taplick, P. Loidl, Biochemistry 38 (1999) 6769–6773.
[25] T. Lechner, A. Lusser, A. Pipal, G. Brosch, A. Loidl, M. Goralik-Schramel, R. Sendra, S. Wegener, J.D. Walton, P. Loidl, Biochemistry 39 (2000) 1683–1692.
[26] G. Brosch, E.I. Georgieva, G. Lopez-Rodas, H. Lindner, P. Loidl, The Journal of Biological Chemistry 267 (1992) 20561–20564.
[27] G. Brosch, M. Goralik-Schramel, P. Loidl, FEBS Letters 393 (1996) 287–291.
[28] M. Curtin, K. Glaser, Current Medicinal Chemistry 10 (2003) 2373–2392.
[29] A. Mai, S. Massa, R. Pezzi, S. Simeoni, D. Rotili, A. Nebbioso, A. Scognamiglio, L. Altucci, P. Loidl, G. Brosch, Journal of Medicinal Chemistry 48 (2005) 3344–3353.
[30] M. Pastor, G. Cruciani, I. McLay, S. Pickett, S. Clementi, Journal of Medicinal Chemistry 43 (2000) 3233–3243.
[31] P.J. Goodford, Journal of Medicinal Chemistry 28 (1985) 849–857.
[32] L. Afzelius, C.M. Masimirembwa, A. Karlen, T.B. Andersson, I. Zamora, Journal of Computer-Aided Molecular Design 16 (2002) 443–458.
[33] K. Abe, K. Amako, Y. Arai, Y. Asano, M. Chiba, Y. Chiba, M. Daigo, T. Emura, I.I. Endo, M. Fukawa, T. Fukui, Y. Fukushima, J. Haba, D. Haidt, I.I. Hayashibara, Y. Hemmi, M. Higuchi, T. Hirose, Y. Hojyo, Y. Homma, Y. Hoshi, Y. Ikegami, N. Ishihara, T. Kamitani, N. Kanematsu, J. Kanzaki, R. Kikuchi, T. Kondo, T. Koseki, K. Kubo, H. Kurashige, T. Matsui, M. Minami, K. Miyake, S. Mori, Y. Nagashima, T. Nakamura, I.I. Nakano, S. Odaka, K. Ogawa, T. Ohama, T. Ohsugi, A. Ono, H. Osabe, H. Saito, H. Sakae, H. Sakamoto, S. Sakamoto, M. Sakano, M. Sakuda, N. Sasao, M. Sato, M. Shioden, J. Shirai, F. Suekane, S. Sugimoto, T. Sumiyoshi, Y. Suzuki, Y. Takada, F. Takasaki, A. Taketani, N. Tamura, R. Tanaka, K. Tobimatsu, Physical Review Letters 61 (1988) 915–918.
[34] O. Lund, M. Nielsen, C.P.W. Lundegaard, in: CASP5, vol. A102, 2002.
[35] J.R. Somoza, R.J. Skene, B.A. Katz, C. Mol, J.D. Ho, A.J. Jennings, C. Luong, A. Arvai, J.J. Buggy, E. Chi, J. Tang, B.C. Sang, E. Verner, R. Wynands, E.M. Leahy, D.R. Dougan, G. Snell, M. Navre, M.W. Knuth, R.V. Swanson, D.E. McRee, L.W. Tari, Structure 12 (2004) 1325–1334.
[36] H.M. Berman, T. Battistuz, T.N. Bhat, W.F. Bluhm, P.E. Bourne, K. Burkhardt, Z. Feng, G.L. Gilliland, L. Iype, S. Jain, P. Fagan, J. Marvin, D. Padilla, V. Ravichandran, B. Schneider, N. Thanki, H. Weissig, J.D. Westbrook, C. Zardecki, Acta Crystallographica 58 (2002) 899–907.
[37] D.A. Pearlman, D.A. Case, J.W. Caldwell, W.S. Ross, I. Cheatham, E. Thomas, S. DeBolt, D. Ferguson, G. Seibel, P. Kollman, Computer Physics Communications 91 (1995) 1–41.
[38] D.F. Wang, O. Wiest, P. Helquist, H.Y. Lan-Hargest, N.L. Wiech, Journal of Medicinal Chemistry 47 (2004) 3409–3417.
[39] D.S. Goodsell, G.M. Morris, A.J. Olson, Journal of Molecular Recognition 9 (1996) 1–5.
[40] A. Mai, M. Esposito, G.S.M. Sbardella, Organic Preparations and Procedures International 33 (2001) 391–394.
[41] G. Brosch, A. Lusser, M. Goralik-Schramel, P. Loidl, Biochemistry 35 (1996) 15907–15914.
[42] D. Kolle, G. Brosch, T. Lechner, A. Lusser, P. Loidl, Methods (San Diego, Calif) 15 (1998) 323–331.
[43] T. Lechner, A. Lusser, G. Brosch, A. Eberharter, M. Goralik-Schramel, P. Loidl, Biochimica et Biophysica Acta 1296 (1996) 181–188.
[44] F. Mohamadi, N.G.J. Richards, W.C. Guida, R. Liskamp, M. Lipton, C. Caufield, G. Chang, T. Hendrickson, W.C.J. Still, Computer and Chemistry 11 (1990) 440–467.
[45] H. Berman, K. Henrick, H. Nakamura, Natural Structural Biology 10 (2003) 980.
[46] H.M. Berman, J. Westbrook, Z. Feng, G. Gilliland, T.N. Bhat, H. Weissig, I.N. Shindyalov, P.E. Bourne, Nucleic Acids Research 28 (2000) 235–242.
[47] M.S. Finnin, J.R. Donigian, A. Cohen, V.M. Richon, R.A. Rifkind, P.A. Marks, R. Breslow, N.P. Pavletich, Nature 401 (1999) 188–193.
[48] F. Fontaine, M. Pastor, F. Sanz, Journal of Medicinal Chemistry 47 (2004) 2805–2815.
[49] G. Cruciani, P. Benedetti, G. Caltabiano, D.F. Condorelli, C.G. Fortuna, G. Musumarra, European Journal of Medicinal Chemistry 39 (2004) 281–289.
[50] A.W. Schuttelkopf, B.M. Aalten, Acta Crystallogr. D Biol. Crystallogr. 60 (2004) 1355–1363.